

CHAPTER 4

THE MECHANICS OF SOFT COHESIVE SEDIMENTS DURING EARLY DIAGENESIS

Bernard P. Boudreau,¹ Mark Barry,¹ Christopher L'Esperance,² Christopher K. Algar³ and Bruce D. Johnson⁴

¹Dalhousie University, Halifax, NS, Canada; ²Satlantic LP, Halifax, NS, Canada; ³Marine Biology Laboratory, Falmouth, MA, USA; ⁴Pro-Oceanus Systems, Bridgewater, NS, Canada

4.1 INTRODUCTION

Natural, surficial, cohesive¹ (clay-bearing), aquatic sediments are subject to a variety of phenomena in which physics, rather than say chemistry, plays an essential role; this includes, but is not limited to, bioturbation, self-weight compaction and phase growth. Scientific monographs (e.g., Berner, 1971, 1980; Boudreau, 1997; DiToro, 2001; Burdige, 2006; Schultz and Zabel, 2006) that focus on early diagenesis, i.e., those changes occurring in the top 1–10 meters (m) of aqueous sediments, make only passing reference to the physics of early diagenetic phenomena. In contrast, civil engineers, soil physicists and geophysicists have afforded great attention to the physics/mechanics of compaction, particularly in soils, anthropogenic sediments and basin-scale studies (e.g., Yong and Warkentin, 1966; Giles, 1997; Wang, 2000; Craig, 2004; Mitchell and Soga, 2005; Das, 2008); yet, this knowledge has not been effectively transferred to obtain a better understanding of early diagenesis.

To place this gap in context, consider the following two questions. Firstly, could one hope to make sense of the flight of a bird without an understanding of the properties of the air it flies in? Likewise, would one be able to predict currents in a stream or the sea without knowledge of the properties and physics of water? Presumptions aside, we would say no in both cases. Yet, most scientists, and even some engineers, who study early diagenetic phenomena have been surprisingly content to ignore the physics of surficial, cohesive sediments.

This chapter addresses the physics of surficial, aqueous, cohesive (clay-bearing) sediments and how these physics play into a number of natural diagenetic phenomena. These phenomena occur in both pristine and contaminated sediments. This chapter is neither extensive nor comprehensive; it simply states a simple version of the three-dimensional, mathematical theory of stresses and strains common to books on mechanics (fluid or solid). Instead, its emphasis centers on some final results from theory and certain applications. As such, while this chapter may appear mathematically unsophisticated to those with a background in mechanics, the aim is to illustrate the application of theory to early diagenesis in natural, cohesive, surficial, soft sediments. Other more mathematical treatments of this topic for surficial sediments are available in Verreert and Berlamont (1988) and Winterwerp and van Kesteren (2004).

¹ We use “cohesive” in the physics sense of “the sticking together of particles,” without the geological restriction that these sediments be muds. Thus, we have found that clay-bearing sands are often cohesive, and are treated that way.

The chapter begins with a review of the conceptual framework for describing the physical behavior of materials subject to stress(es). This review introduces names for certain end-member behaviors and the parameters found in their mathematical descriptions. Obtaining values of these constants for soft clay-bearing sediments is not a trivial task and a subsequent section reviews progress in that direction. Finally, these behavioral concepts are used to explain self-weight compaction, animal motion and bioturbation, and bubble formation – all early diagenetic phenomena that occur in pristine and contaminated sediments. Such phenomena are relevant to the study and understanding of contaminated sediments because compaction can concentrate pollutants, bioturbation can spread the contaminant to pristine zone and areas, and bubbles can release volatiles chemicals to the overlying waters.

4.2 PHYSICAL MODELS (RHEOLOGY) OF MATERIALS

4.2.1 Conceptual Models

If a stress (force per unit area), σ , is applied to a homogeneous material, a number of outcomes are possible. The application of stress usually engenders strains (deformations), ϵ , in the material. Stress and strain are inherently three-dimensional quantities (i.e., tensors), and they are defined mathematically in a subsequent Section 4.2.5. For the moment, however, they can be treated as uni-dimensional, which can then be simply extended to three dimensions.

Common classic responses to stress include (Long, 1961; Shames, 1964; Jaeger, 1969; Davis and Selvadurai, 1996, 2002; Giles, 1997; Winterwerp and van Kesteren, 2004; Bird et al., 2007):

- Continuous deformation of the material with time ($\dot{\epsilon} = d\epsilon/dt \neq 0$) as long as the force is applied (Figure 4.1a).² This type of response characterizes what is known as a fluid; hence the common adage thrown at generations of first year physics students that “a fluid does not support a stress.” If the rate of strain (deformation) is constant with time, the fluid is termed Newtonian. Non-Newtonian fluids include power-law fluids and Bingham plastics.
- A material can adopt a new stable (time-independent) configuration upon application of a stress. If this deformation is entirely reversible when the stress is removed, then this material is said to be elastic (Figure 4.1b). If the new configuration is stable, but not reversible, the stress has passed the Yield or Elastic Limit and has deformed plastically. Plastic deformation can involve a flow. Strain hardening describes stable, increasing deformation that is significantly irreversible.
- Some materials will exhibit fluid-like behavior in response to some stresses and stress rates, while elastic or even plastic behavior for others. These are visco-elastic and visco-elasto-plastic materials. Sediments fall within this category, but idealization to an end-member is often possible.

The above classification is not exhaustive, and it is primarily based on tensional (pulling) stresses on solids. Geological processes are often compressive and that is considered below.

² Many papers in the literature plot strain, ϵ , or strain rate (velocity), $\dot{\epsilon}$, on the x-axis, probably for historic reasons, i.e., you could see the strains or strain rates, but stresses were hard to measure. Figure 4.1 plots the stress, σ , on the x-axis to be consistent with the scientific tradition of placing the independent variable (cause) on the abscissa. There will be an advantage to this when we consider compaction.

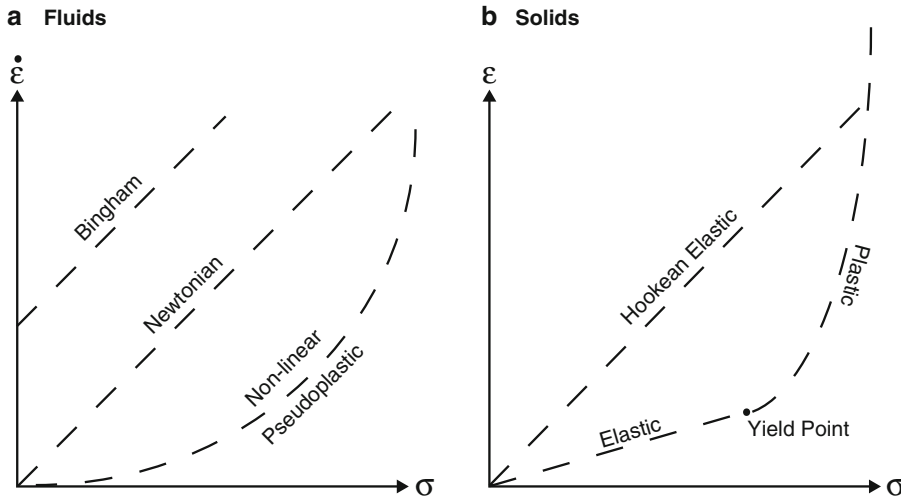


Figure 4.1. Figures illustrating classic behavior of fluids (a) and solids (b) to applied stress (σ). (a) True fluids do not support stresses and flow as a result of applied stress, i.e., their strain changes continuously with time, $\dot{\epsilon}$. The flow response may be linear (Newtonian) or nonlinear (e.g., pseudoplastic). A Bingham fluid acts like a solid at low stresses, but as a Newtonian fluid above a threshold. (b) Elastic solids will reach a new equilibrium configuration, characterized by the strain ϵ , under applied (tensile) stress. If the deformation is completely reversible and linear, then the solid is Hookean. At some stress the material deformation will cease to be reversible (yield point), and further deformation is termed plastic. Note that a solid may deform linearly with applied stress, but fail to be reversible; plasticity does not necessitate nonlinearity.

4.2.2 Phenomenological Formulas and Constants

The behaviors described above can be encapsulated into simple behavioral formulas, so-called constitutive equations, e.g., Jaeger (1969) and Davis and Selvadurai (1996, 2002). In general, stress applied even in a single direction will create strains in all directions; nevertheless, it is possible to discuss constitutive equations by considering only tensile/compressive stress applied in a single direction, σ , and the resulting deformation in that direction, ϵ (see Appendix 4A).

A fluid deforms continuously with applied stress (e.g., a pressure gradient), and a Newtonian fluid does so linearly; thus, the latter is characterized by the formula

$$\sigma = \eta \dot{\epsilon} \quad (\text{Eq. 4.1})$$

where η is the dynamic viscosity. By equating $\dot{\epsilon}$ to the spatial gradient of the velocity, one obtains the more familiar form of Newton's law of viscosity (Bird et al., 2007).

A linear elastic (Hookean) substance responds reversibly to stresses to attain a new equilibrium configuration, i.e.,

$$\sigma = k \epsilon \quad (\text{Eq. 4.2})$$

where k is formally the “spring constant,” but it is identical to Young's modulus, E , for the purposes in this chapter, i.e., $E = k$. The models advanced by Johnson et al. (2002), Gardiner et al. (2003) and Algar and Boudreau (2009) to explain methane bubble formation in muddy sediments are Hookean (see below).

There are a variety of idealized materials that exhibit elastic behavior at low strains and fluid behavior above a strain threshold. When a solid behavior is Hookean below such a limit and the subsequent fluid behavior is Newtonian, then the substance is termed a Bingham plastic. Bingham models have been applied to many sediments (see the review by Verreert and Berlamont (1988)).

A Kelvin or Voigt material, which is one form of a linear visco-elastic substance, is approximated by assuming that viscous and elastic behaviors act in parallel, i.e.,

$$\eta \dot{\epsilon} + E\epsilon = \sigma \quad (\text{Eq. 4.3})$$

and this has been employed by Maa and Mehta (1988) and Jiang and Mehta (1995) to describe the transport behavior of some muds, and by Algar (2009) to explain gas bubble rise in cohesive sediments. Conversely, a Maxwell substance assumes that these responses act in series, i.e.,

$$\dot{\epsilon} = \left(\frac{\dot{\sigma}}{E} \right) + \left(\frac{\sigma}{\eta} \right) \quad (\text{Eq. 4.4})$$

and this has been employed in modeling fluidized muds (Maa, 1986; Williams and Williams, 1989). Many other types of behavior can be captured by these types of simple constitutive equations.

As noted above, a solid may exhibit plastic behavior, during which the solid will deform as in elastic deformation, but the deformation is not reversible; in other words, plastic deformations permanently alter the shape and relative positions of all the “particles” that make up the solid. Release of the stress can lead to some relaxation of the strain, but not to the original undeformed positions. The simplest models of plasticity are unidirectional in terms of the strain obtained for a stress level and can be simple algebraic equations, including linear forms like Equation 4.2. Plasticity is sometimes used to describe compaction of sediments, as discussed below.

4.2.3 Phenomenological Constants for Sediments

While the models described above were originally intended for relatively homogeneous materials, soft, cohesive (clay bearing) sediments, as well as other geological media, have been described using these equations (Jaeger, 1969). Aqueous sediments are patently heterogeneous and composite, made of an immiscible mixture of pore fluid and solid grains. When subject to a stress, sediments can and do behave in a more complex manner than homogeneous substances, and this in turn complicates not only their classification, but the values and meanings of their phenomenological constants.

Applying a stress can cause pore fluid to move relative to the solid grains, i.e., Darcy flow. If flow does occur, the solids and fluids are usually displaced relative to each other; therefore, this separation would characterize an irreversible deformation. As a consequence, scientists and engineers who make measurements of the geo-mechanical properties of sediments and the resulting phenomenological constants are careful to specify if the measurement permitted or did not permit pore fluid flow, regardless of whether or not such a relative displacement/flow, in fact, did occur. Thus, if the excess porewater pressure can be dissipated by flow, the measurement is termed drained; conversely, if pore fluid flow is prevented, e.g., by confinement in an encompassing, impermeable sample container, then the measurement is called undrained. Sediments in nature are usually in a drained state with respect to natural processes, so that drained-state elastic and plastic constants would normally be employed.

Values for the viscosity (η) and the true/reversible Young’s modulus (E) have been obtained experimentally for a number of sediment sites; these values, as well as some

Table 4.1. Selected Experimentally Determined Viscosities of Some (Non-resuspended) Muds and Other Reference Materials

Source Location	Porosity	Viscosity (Pa·s)	Source
Kerala, India	0.88	2.76×10^4	Jiang and Mehta, 1995
Okeechobee, USA	0.89	9.56×10^2	Ibid
Mobile Bay, USA	0.87–0.93	$0.0215\text{--}2.24 \times 10^2$	Ibid
Synthetic mud	0.89–0.97	1.15×10^4	Ibid
Gulf of Mexico	n/a	5.0×10^4	Hsiao and Shemdin, 1980
Pure water (20°C)	–	1.0×10^{-3}	http://en.wikipedia.org/wiki/Viscosity
Molasses (25°C)	–	5.0–10	Ibid
Peanut butter (25°C)	–	250	Ibid

environmental information, are provided in Tables 4.1 and 4.2. It is not known if these values are representative of all cohesive sediments, nor is the dependence of these values on sediment properties, i.e., depth, grain size, porosity, temperature, organic matter content, etc., quantitatively established at this time. The few sediment viscosities in Table 4.1 are for non-fluidized conditions. The values show that clay-bearing sediment is indeed “slower than molasses in winter”³ and peanut butter on cold toast! This small viscosity explains why clays removed from core barrels retain their shape under their own weight (load) for long periods of time; nevertheless, under suitable stress conditions sediments can and do flow, to which turbidite flows attest.

Reversible (elastic) Young’s moduli are reported in Table 4.2 and require one caveat. Finite-strain E values from reversible compression/release tests, e.g., Figure 4.2, are on the order of 10^5 Newtons/square meter (Nm^{-2}), or up to five orders of magnitude lower than what is recorded by acoustical measurements. This apparent discrepancy is not a problem, but rather it is related to the length and time scales of the applied stress and the measurements (Clayton and Heymann, 2001; L’Esperance, 2009). The two methods measure different parameters; consequently, one should use finite strain values for finite strain phenomena.

The reversible (elastic) E values in Table 4.2 are again from a limited data set from only a few sites, and they can hardly be called representative. In addition, the dependence of the reversible E on sediment properties and depth is not well known, but it does appear to increase with depth (Barry, 2010). See as an example Figure 4.3, i.e., the sediment becomes increasingly stiff with depth, undoubtedly due to the effects of compaction. More determinations from a wide variety of cohesive sediment environments are needed.

Another mechanical parameter that will appear in subsequent formulas is Poisson’s Ratio, ν ; this parameter is the ratio of the deformation in the direction of an applied uni-axial stress to the resulting deformation in the other directions (assuming isotropy). For an incompressible solid, $\nu = 0.5$. Since both water and most solids that make up sediments are incompressible, one would expect a ν near 0.5, at least if the sediment is fully saturated. Table 4.3 contains Poisson’s Ratios for various sediments (including some sands), and the expectation is generally met. Even acoustically determined ν values are near 0.5. However, the presence of significant

³ Old North American proverb, indicating very slow to the eye.

Table 4.2. Young's Modulus Values (Drained) for Various Sediments and for Selected Reference Materials

Source Location	Sediment Type	E (Pa) ^a	Method	Source
Cole Harbour, NS	Silty sand	$2.4\text{--}5.0 \times 10^4$	Uniaxial compression	L'Esperance, 2009
Cole Harbour, NS	Silty sand	1.4×10^5	Uniaxial compression	Johnson et al., 2002
Windsor and Canard, NS	Clay-bearing silty sands	$0\text{--}9 \times 10^5$ (0–25 cm)	<i>In situ</i> dilatometer	Barry, 2010
Continental shelf	Fine sand to silty sand	$8.13\text{--}15.11 \times 10^8$	Acoustic (calculated)	Hamilton, 1971
Windsor, NS	Silt to clay	7.5×10^5	Uniaxial compression	L'Esperance, 2009
Continental shelf	Silt to clay	4×10^8	Acoustic (calculated)	Hamilton, 1971
Deep sea	Clays	$1.45\text{--}4.3 \times 10^8$	Acoustic (calculated)	Hamilton, 1971
London clay (terrestrial)	Clay	$1.1\text{--}1.2 \times 10^8$	Bender element-triaxial	Gasparre et al., 2007
Margin sediment, India	?	$2.5\text{--}2.9 \times 10^9$	Acoustics	Raju and Ramana, 1986
Synthetic	Gelatin ^b	$0.6\text{--}1.3 \times 10^3$	Uniaxial compression	Takada, 1990
Synthetic	Gelatin ^b	$2.5\text{--}50 \times 10^3$	Uniaxial compression	Hall et al., 1997
Synthetic	Gelatin ^b	$1.5\text{--}10 \times 10^3$	Uniaxial compression	Johnson et al., 2002
Synthetic	Gelatin ^b	$31\text{--}81 \times 10^3$	1-D tensile tester	Sato et al., 2001
Synthetic	Gelatin ^b	$9.7\text{--}17 \times 10^3$	Uniaxial compression	L'Esperance, 2009
Synthetic	Polyethylene	$0.8\text{--}2.7 \times 10^9$	Compression	Johnson et al., 2002
Synthetic	Nylon	$2\text{--}4 \times 10^9$	Compression	Johnson et al., 2002
Synthetic	Rubber	$0.01\text{--}0.1 \times 10^9$	Compression	http://www.engineeringtoolbox.com/young-modulus-d_417.html
Synthetic	Aluminum	69×10^9	Compression	http://www.engineeringtoolbox.com/young-modulus-d_417.html

^a1 N m⁻² = 1 Pa

^bVaries considerably with mixture strength and temperature

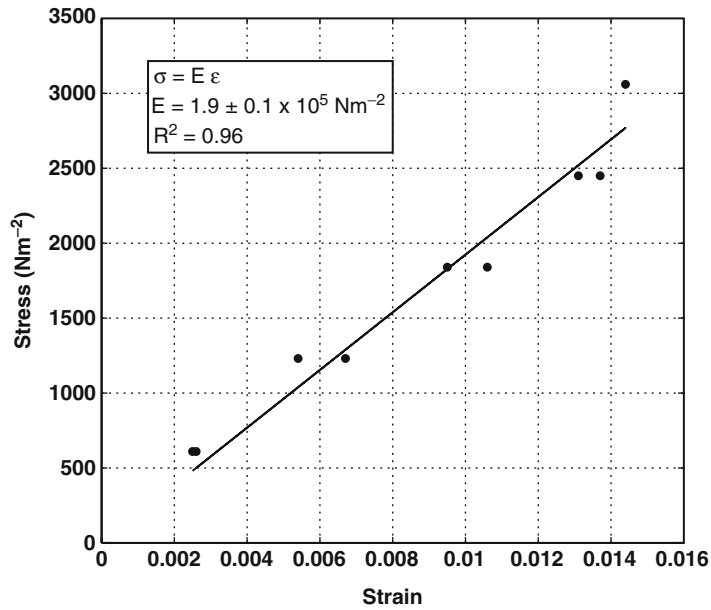


Figure 4.2. An example of a linear and reversible stress-strain diagram for a cohesive sediment from Nova Scotia, Canada. This is true Hookean elasticity with a Young’s modulus of $1.9 \times 10^5 \text{ Nm}^{-2}$ (from Barry, 2010).

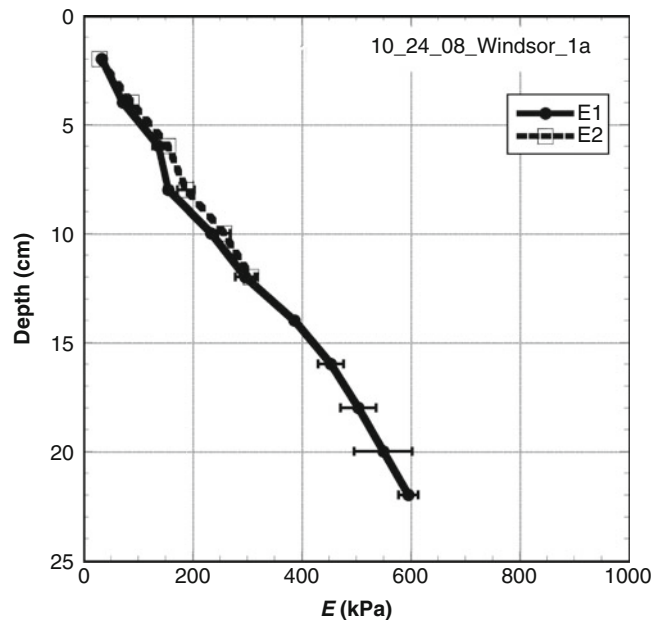


Figure 4.3. Typical depth profile of (reversible) Young’s modulus, E , at a field site (Windsor) in coastal sediment of the Bay of Fundy, Nova Scotia, Canada. There is an essentially linear increase in modulus with depth from values near zero at the surface to values of 600 kPa at 22 cm depth. Profiles were run in two adjacent locations only 30 cm apart (*solid* and *dashed lines*) and show good homogeneity over short, lateral distances. One standard deviation error shown for average of three measurements (from Barry, 2010, but also see similar plots in Barry et al., 2012).

Table 4.3. Poisson's Ratio (Drained) for Various Sediments

Source Location	Sediment Type	ν (dimensionless)	Source
Various	Sand, fine sand, silty sand	0.453–0.491	Hamilton, 1971
San Diego	Medium sand	0.494	Hamilton et al., 1970 as cited in Hamilton, 1979
Shallow to deep sea	Silt clays, turbidites and mudstones	0.420–0.497	Hamilton, 1979
North sea	Sand	0.487–0.499	Hamilton, 1979
Cole Harbour, NS	Fine sand	0.49956 ± 0.003	L'Esperance, 2009
Deep sea to continental terrace	Silty clay	0.478–0.487	Hamilton, 1971
–	Clays	0.4982–0.4997	Davis and Schulteiss, 1980 as cited in Salem, 2000
Windsor, NS	Silt/clay	0.4989 ± 0.0008	L'Esperance, 2009
–	"Typical" silt and clay	0.25	Breitzke, 2006
Various	Soils (including undersaturated)	–1.0 to 0.5	Pickering, 1970 as quoted by Salem, 2000
Synthetic	Gelatin	0.5	Markidou et al., 2005

free gas can drive ν down to smaller values, even negative values. Some geophysicists employ ν values between 0.2 and 0.3 for some acoustical calculations, but measurements tend to support values near 0.5 when gas is not present.

Given Young's modulus and Poisson's Ratio, it is possible to calculate two other common elastic constants, the shear modulus, G , (Davis and Selvadurai, 1996, 2002)

$$G = \frac{E}{2(1 + \nu)} \quad (\text{Eq. 4.5})$$

and the Lamé constant, λ ,

$$\lambda = \frac{\nu E}{(1 + \nu)(1 - 2\nu)} \quad (\text{Eq. 4.6})$$

If sediment is essentially incompressible, as indicated by the values in Table 4.3, then the shear modulus is $E/3$ and the Lamé constant is infinite. Finite-strain bending plate measurements (e.g., Lavoie et al., 1996) produce G values of $3\text{--}4 \times 10^5 \text{ Nm}^{-2}$ going from a depth of 20 centimeters (cm) to 200 cm in a muddy sediment of Ekernfjorde Bay (Germany). If Windsor-Canard sediments (Table 4.3) are indicative of E values for similar sediments, then one would indeed predict G values in this range, if these sediments are incompressible; therefore, the existing database of non-acoustic shear moduli may represent a significant resource for obtaining values of (reversible) Young's moduli for aqueous sediments.

If sediment can act as a solid, at least under some stress conditions, then it can fail, i.e., fracture, rather than simply flow or plastically deform. For example, fracture of sediments occurs when bubbles form as a result of gas injection (Johnson et al., 2002) or when various organisms (worms, clams, etc.) move through soft cohesive sediments (Dorgan et al., 2005).

Table 4.4. Fracture Toughness (K_{IC}) of Some Cohesive Sediments

Source Location	Sediment Type	K_{IC} ($N\ m^{-3/2}$)	Source
Cole Harbour, NS	Clay-bearing silty sand	410–550	Johnson et al., 2002
Canard, NS	Clayey silt	80–1,300	Johnson et al., 2012
Various	Agricultural soils	1,503–6,036	Aluko and Chandler, 2006
Synthetic	Gelatin	45–110 ^a	Menard and Tait, 2002
Synthetic	Gelatin	28–60 ^a	Rivalta and Dahm, 2006

^aDependent on concentration and temperature

The simplest theory of solids, i.e., linear elastic fracture mechanics (LEFM), e.g., Broek (1982) or Gross and Seelig (2006), characterizes the fracture strength of a solid by a parameter K_{IC} , known as the fracture toughness or the critical stress intensity factor – a real mouthful. K_{IC} is a material property and it has been measured in a few soft cohesive sediments, as well as in the analogue material, gelatin (see Table 4.4). Fracture of real solids is related to K_{IC} , rather than tensile strength, because real solids contain flaws, and it is the opening of these flaws that permits initiation of fracture. In an ordered solid, such as a perfect crystal that contains no flaws, fracture must break the underlying bonds of the structure, and that takes far more energy, characterized as the tensile strength.

That cohesive sediments have a fracture toughness should come as no surprise, as they have long been credited with possessing shear strength (e.g., Mehta and Partheniades, 1982; Partheniades, 1991), which is simply fracture by applied shear, rather than tensional, forces. (Note that while such measurements are reported as shear strength, they are, in fact, measurements of shear toughness.) Measurements of shear strength have long been made in cohesive sediments, and the literature on that topic is so large that it cannot be even superficially reviewed here. Shear strength is employed as a critical parameter in modelling the erosion of mud beds. The relationship between shear strength and K_{IC} has not been established for sediments.

The parameter K_{IC} appears generally to increase with depth due to compaction (Johnson et al., 2012), as does the shear strength (Partheniades, 1991), but K_{IC} is also dependent on grain size of the sediment, and probably on other sediment properties and may thus change with an alteration in lithology (Figure 4.4). Sands have no, or little, cohesion, while clays do; thus, sandier sediment layers show up as drops in K_{IC} values in profiles that otherwise increase with depth, again due to compaction.

4.2.4 The Origin of Sediment Mechanical Properties

The value of the mechanical constants for a cohesive sediment must be related to the way this material is put and held together. Early views of cohesive sediment fabric (e.g., Englehardt and Gaida, 1963; Rieke and Chilingarian, 1974) centered on the idea of the presence a “house of cards” structure of fine clay platelets, held together by the attraction of positively charged edges to negatively charged basal plates. TEM photomicrographs of real cohesive sediments (see Bennett et al., 1991, 1996) show a more complicated fabric, with mixtures of particles of different shape and sizes, clays both stacked and in house of cards and with admixed organic matter. In fact, while electrostatics plays a role in aggregation of sediments, these sediments seem to be primarily held together by long polymer organic molecules (e.g., Hunter, 2001; Winterwerp and van Kesteren, 2004). An indication of the truth of that hypothesis is contained in

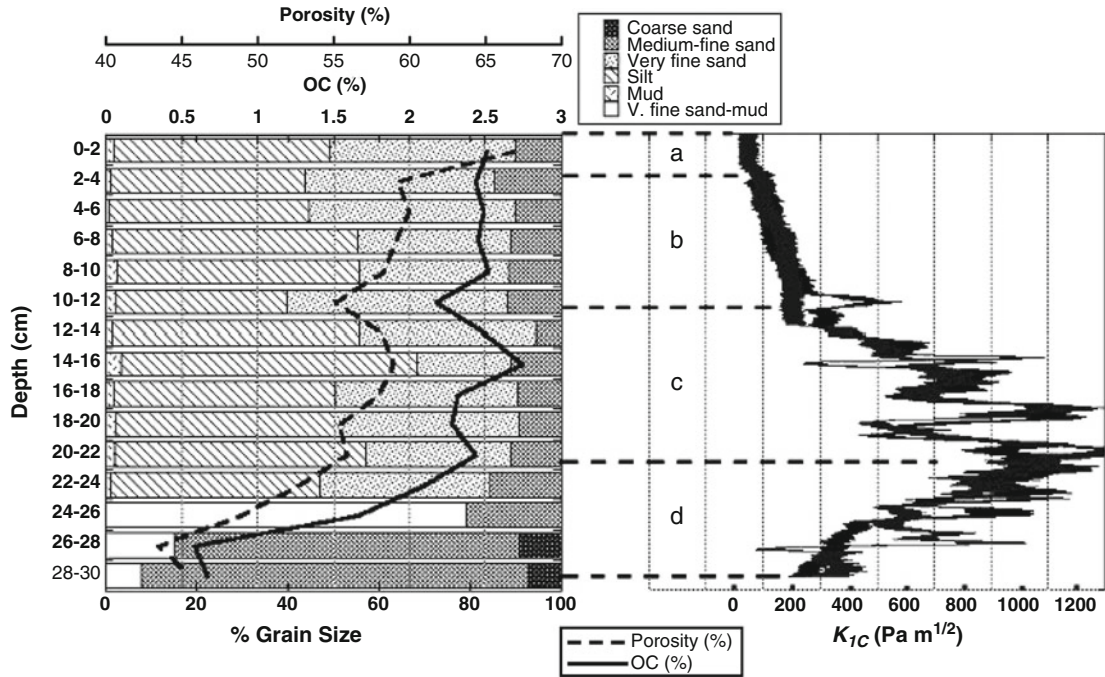


Figure 4.4. The *in situ* fracture toughness (K_{1C}) of a sediment from the Bay of Fundy, Nova Scotia, Canada, as a function of depth and correlated to grain size of the sediment with depth. Generally, K_{1C} increases with depth due to compaction, but the appearance of sand below 22 cm causes a drop in K_{1C} (data in this figure are reported in Johnson et al., 2012).

Table 4.2, which shows that gelatin, made of long chain polymeric proteins, has a Young's modulus similar to that of sediments. Similarly, the fracture strength of sediments and gelatin are comparable (Table 4.4), which suggests the breaking of similar bonds.

4.2.5 The Mechanical Equations for a Deforming Body

Now that we have the mechanical models and constants relevant to sediments, how are they employed? These constitutive equations and their associated constants form part of a system of equations that govern the deformation of any material. An example set of such equations is given below for an elastic Hookean substance, which is the most commonly assumed form. In this example, we generalize to a three-dimensional Cartesian coordinate system.

The following equations govern the interplay between the applied stresses and the observed deformations. There are nine possible stress components, but isotropic symmetry requirements reduce this to six independent components, σ_x , σ_y , σ_z , τ_x , τ_y and τ_z , where σ indicates a normally directed stress and τ represents a tangential (shear) stress. The subscripts on σ correspond to the direction in which the normal stress is applied and the subscripts on τ indicate the direction normal (perpendicular) to the plane on which the tangential stress is applied.

For a homogeneous solid, these stresses must satisfy the so-called static equilibrium conditions (e.g., Timoshenko and Goodier, 1934; Biot, 1941; Davis and Selvadurai, 1996)

$$\frac{\partial \sigma_x}{\partial x} + \frac{\partial \tau_z}{\partial y} + \frac{\partial \tau_y}{\partial z} - b_x = 0 \quad (\text{Eq. 4.7})$$

$$\frac{\partial \tau_z}{\partial x} + \frac{\partial \sigma_z}{\partial y} + \frac{\partial \tau_x}{\partial z} - b_y = 0 \quad (\text{Eq. 4.8})$$

$$\frac{\partial \tau_y}{\partial x} + \frac{\partial \tau_x}{\partial y} + \frac{\partial \sigma_z}{\partial z} - b_z = 0 \quad (\text{Eq. 4.9})$$

where the b_i ($i = x, y, z$) are the components of any relevant body force (e.g., gravity).

The other observable is the amount of displacement of any arbitrary point in the solid due to the application of the stress(es), denoted u , v and w for the components in the x , y , and z directions. The strains in the constitutive equations are defined from the displacements as (e.g., Timoshenko and Goodier, 1934; Biot, 1941; Davis and Selvadurai, 1996)

$$\varepsilon_x = \frac{\partial u}{\partial x} \quad (\text{Eq. 4.10})$$

$$\varepsilon_y = \frac{\partial v}{\partial y} \quad (\text{Eq. 4.11})$$

$$\varepsilon_z = \frac{\partial w}{\partial z} \quad (\text{Eq. 4.12})$$

$$\gamma_x = \frac{\partial w}{\partial y} + \frac{\partial v}{\partial z} \quad (\text{Eq. 4.13})$$

$$\gamma_y = \frac{\partial u}{\partial z} + \frac{\partial w}{\partial x} \quad (\text{Eq. 4.14})$$

$$\gamma_z = \frac{\partial v}{\partial x} + \frac{\partial u}{\partial y} \quad (\text{Eq. 4.15})$$

where ε_i is the normal strain (compression or dilation) and γ_i is the tangential or shear strain (for $i = x, y, z$).

Finally, the stresses and strains are related through so-called compatibility equations, which implement the constitutive equations. For a Hookean solid, these read (e.g., Timoshenko and Goodier, 1934; Biot, 1941; Davis and Selvadurai, 1996; Wang, 2000)

$$\varepsilon_x = \frac{\sigma_x}{E} - \frac{\nu}{E}(\sigma_y + \sigma_z) \quad (\text{Eq. 4.16})$$

$$\varepsilon_y = \frac{\sigma_y}{E} - \frac{\nu}{E}(\sigma_x + \sigma_z) \quad (\text{Eq. 4.17})$$

$$\varepsilon_z = \frac{\sigma_z}{E} - \frac{\nu}{E}(\sigma_x + \sigma_y) \quad (\text{Eq. 4.18})$$

$$\gamma_x = \frac{\tau_x}{G} \quad (\text{Eq. 4.19})$$

$$\gamma_y = \frac{\tau_y}{G} \quad (\text{Eq. 4.20})$$

$$\gamma_z = \frac{\tau_z}{G} \quad (\text{Eq. 4.21})$$

where E is Young's modulus (Table 4.2), G is the shear modulus, and ν is Poisson's ratio (Table 4.3), as defined above. Equations 4.7, 4.8, 4.9, 4.10, 4.11, 4.12, 4.13, 4.14, 4.15, 4.16, 4.17, 4.18, 4.19, 4.20, and 4.21 define a system of 15 equations in 15 unknowns; these equations have been solved analytically for some cases, but are readily solved numerically, including by commercial packages,

such as COMSOL. Plasticity may sometimes be described using a Hookean model, as long as one does not attempt to unload the solid using the same constitutive equation(s).

Biot (1941, 1956) extended these equations to a composite porous medium, such as sediment, in which the pore fluid may separate from the solid matrix of particles. Equations 4.16, 4.17, and 4.18 gain in that case a new term each that accounts for the “increment of water pressure”; this term disappears in drained situations. In addition, as the porosity or “variation in water content” becomes a variable in this case, another equation for changing water content must then be added and its constitutive equation is Darcy’s law. Biot (1973), and many authors thereafter, have extended these equations for porous solids with non-linear constitutive equations and even plasticity (e.g., Small et al., 1976). A short historical review of this topic is available in de Boer (1992).

4.3 MECHANICAL PROCESSES IN NATURAL AQUATIC SEDIMENTS

We now summarize the results of applying mechanical theories to three common diagenetic processes where physics are central to understanding the phenomenon: compaction, bubble growth and bioturbation.

4.3.1 One-Dimensional Compaction with Sedimentation

The quintessential mechanical process during diagenesis is self-weight compaction, or consolidation, with sedimentation of new materials. The accumulating weight of a sediment will cause the porewater, held between sediment grains, to be expelled, creating a decrease in porosity with depth and time.

Models of compaction have a long history in the soils and sediments literature (see the summaries in Giles, 1997; Winterwerp and van Kesteren, 2004). In particular, Terzaghi (1943) produced the first systematic model of compaction by introducing the concept of consolidation/excess pressure that drives the compaction process; this was followed by classic papers from Gibson (1958), McNabb (1960), Been and Sills (1981), Lee and Sills (1981), Koppula and Morgenstern (1982), Znidarcic and Shiffman (1982) and Gibson et al. (1989). Oddly enough, reference to such work is virtually absent in the early diagenetic literature. This absence is in part the result of the unfortunate age-old problem of isolation of fields, but also due to the different perspectives of scientists studying early diagenesis versus those considering soils, or the entire sediment column, or man-produced lumps of sediment.

In this respect, engineers, geophysicists, geotechnical scientists and soil scientists use reference frames that are either fixed to a datum, e.g., the surface of the underlying bedrock, or a selected mass of sediment. The first is a fixed Eulerian frame, while the second is a moving Lagrangian frame. One can, of course, mathematically convert from one to the other, but one choice or the other may be preferred for convenience. Diagenetic studies traditionally do neither; because the focus is on the sediment-water interface, the reference frame is anchored instead at the moving sediment-water interface, i.e., a moving Eulerian coordinate system (e.g., Berner (1980); Boudreau (1997) and Burdige (2006)). This is technically a moving-boundary problem, but by anchoring the coordinate system to the moving sediment-water interface, that problem is transformed into a uni-dimensional problem with a fixed boundary and an apparent velocity (component) of the solids and fluid away from the interface (Berner, 1980; Boudreau, 1997).

Toorman (1996) and Boudreau and Bennett (1999) have formulated the equations of elastic-plastic compaction in this moving diagenetic Eulerian frame. That development will not be presented here. Instead we present solely the distillation and end-result of those studies.

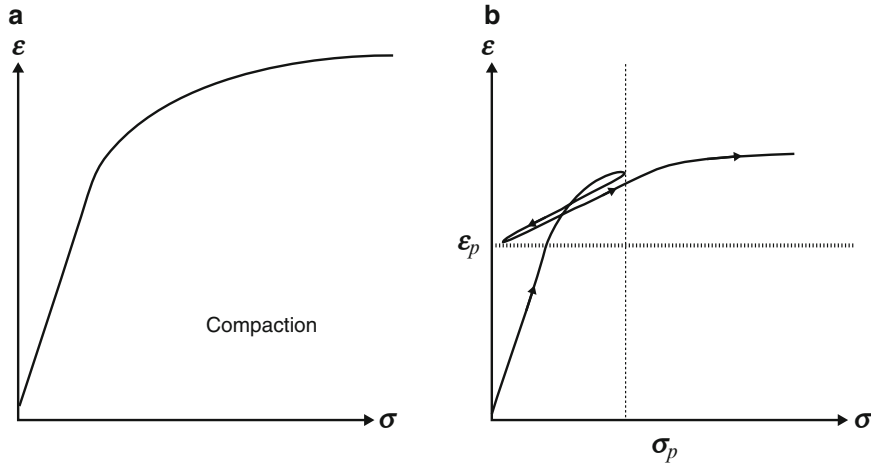


Figure 4.5. (a) An idealized stress-strain curve for a solid under compactive stress. The smaller and smaller effect of stress is due to the increasing difficulty of forcing water out of the sediment structure, and is termed compactive hardening here. (b) This figure illustrates the type of irreversibility expected during compaction, if the load is removed.

If one considers the one-dimensional, steady state compaction of a muddy sediment, an appropriate measure of strain in this case is the relative change in porosity, $\varphi(x)$:

$$\varepsilon_x = \frac{\varphi(x) - \varphi_o}{\varphi_o} = \frac{\varphi_{so} - \varphi_s(x)}{\varphi_o} \quad (\text{Eq. 4.22})$$

where x is the depth from the sediment-water interface (positive), $\varphi_s(x)$ is the solid volume fraction, i.e., $1 - \varphi(x)$, and the subscript o indicates an initial value at $x = 0$.

Next, we need to consider the constitutive behavior of sediments. Compaction is an essentially irreversible process by which porewater is “squeezed” out of sediments (permanently) due to self weight. This means that the process is not truly elastic, and the stress-strain relationship for compaction must reflect this irreversibility. This does not mean that there is not a small truly elastic component to the process, but overall it is a permanent deformation, i.e., plastic. Figure 4.5a illustrates the strain (relative porosity change) as stress (weight) is applied continuously to a sediment sample. There is a linear portion, which may or may not be truly elastic, and a nonlinear portion, which indicates definite plastic behavior. In the non-linear region, it takes progressively more and more weight to produce a constant increment of strain (compaction). The literature does not seem to contain a term for this increasing difficulty to compact (compactive hardening?).

If during non-linear plastic compaction the load is removed at some stress σ_p , then the sample does not return to zero strain, but to a finite level of strain ε_p , which reflects the permanent deformation of the porosity, caused by the removal of water (Figure 4.5b). Recommencing the compaction essentially returns the stress-strain relation to the theoretical curve for that material.

Figure 4.6 illustrates the stress-strain relation in sediments from a core taken on the California Margin (Bennett et al., 1999); these data follow the trend indicated in Figure 4.5a. Boudreau and Bennett (1999) offer a non-linear (irreversible/plastic) stress-strain relation for sediment compaction that is consistent with the above principles, i.e.,

$$\varphi_s = s[1 - e^{-r\sigma}] + \varphi_{so} \quad (\text{Eq. 4.23})$$

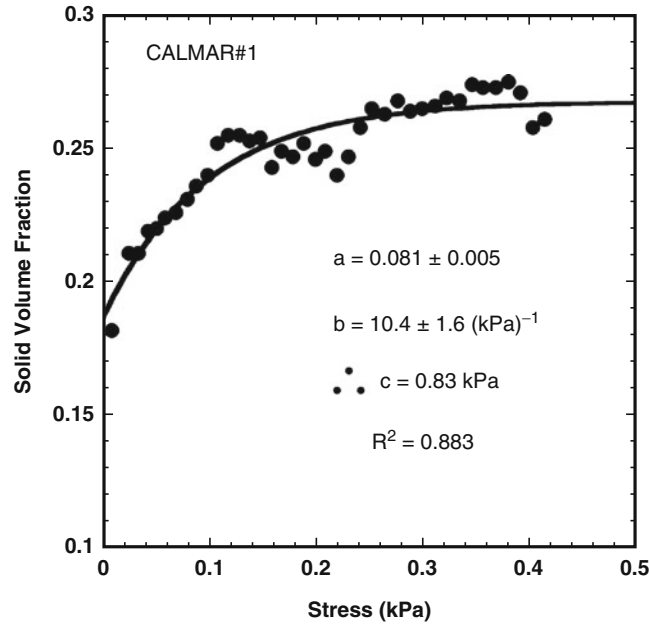


Figure 4.6. A measured solid volume-stress profile from a sediment off the California coast (data taken from Bennett et al., 1999).

where r and s are (empirical) parameters that account for the initial compressibility of the sediment and the attenuation of stress, respectively; a fit of Equation 4.23 is illustrated in Figure 4.6. For small stresses, one can expand the exponential in Equation 4.23 and ignore nonlinear terms; then using Equation 4.22, one can obtain a linear stress-strain relation:

$$\frac{\varphi_{so} - \varphi_s(x)}{\varphi_o} = -c\sigma \quad (\text{Eq. 4.24})$$

where $c = r \cdot s$, which is an apparent Young's modulus for compaction; however, this compaction is irreversible and c is not a true elastic constant.

The calculated value of c for this sediment is 0.83 kilopascal (kPa), which is one to two orders of magnitude smaller than the measured reversible Young's moduli for cohesive sediments in Table 4.2. One should not be shocked by this result; again, time scale of application of the force is the key to the separation of water and solids. Compaction c values are smaller than elastic E values because the forces applied over decades to millennia during *in situ* compaction cause the sediment to adjust (strain) more by expelling water, i.e., plastic deformation.

Porosity and its change with depth affect the chemistry of sediments in at least two ways. Compaction engenders a flow of porewater and that can move solutes; however, during early diagenesis, this flow is often small compared to transport by molecular diffusion, and it is this latter process that feels the effects of compaction. Specifically, diffusion is hindered by the presence of the solids, both because the area for diffusion is reduced and because the path the solutes must traverse is longer (see Berner, 1980; Boudreau, 1997). The longer path-length effect is characterized by the tortuosity, θ , which is the ratio of the length of the mean path that is actually followed to the direct distance. Thus, $D_e = D/\theta^2$, where D_e is the effective diffusion coefficient and D is the diffusion coefficient in the absence of the solid particles.

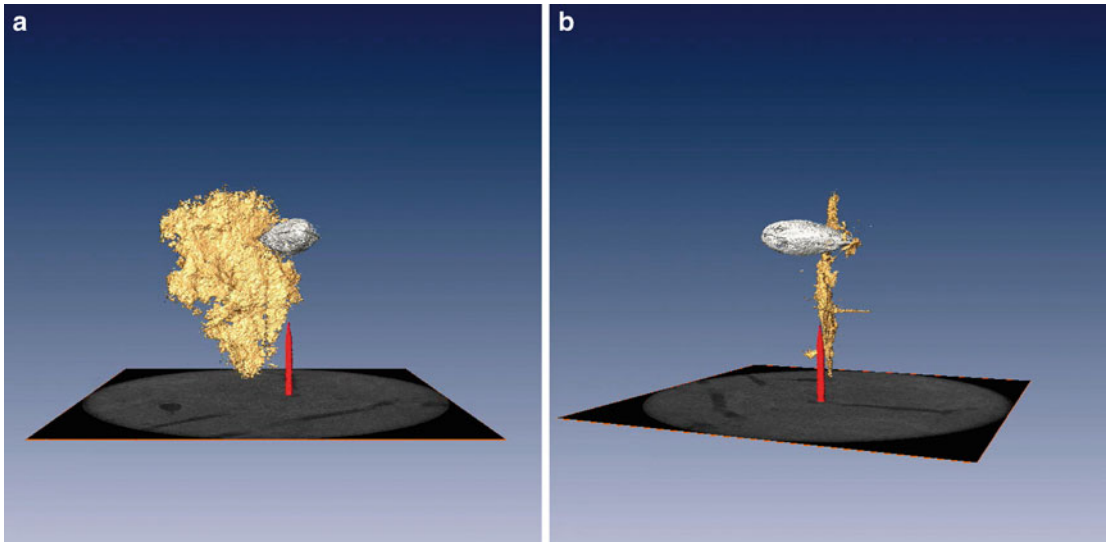


Figure 4.7. Two CT-scans (false color) of a bubble injected into natural sediment. The bubble (gas) is gold, the injector needle is red, and a small mussel shell, in contact with the bubble, is in gray. The sediment itself has been “removed” digitally. The *left-hand* diagram (a) shows a plane view and the *right-hand* (b) a cross section. The bubble is a flat, somewhat irregular mass that is reminiscent of a “corn flake”; for modeling purposes, it is adequately approximated as an eccentric oblate spheroid (from Best et al., 2006, reproduced with the kind permission of the American Geophysical Union).

Amongst others, Boudreau (1996) and Boudreau and Meysman (2006) have analyzed the existing data and presented models of cohesive sediment structure to argue that $\theta^2 = 1 - \ln(\phi^2)$. Therefore, as compaction reduces ϕ , this feeds back strongly into the effective solute diffusivity. This effect is part of all models of diagenetic processes for solutes in sediments.

4.3.2 The Growth of Methane Bubbles

When a new phase, e.g., free gas or an authigenic mineral, grows in sediments, the phase must make room for itself by displacing the sediment or incorporating the sediment. Gas bubbles, usually methane, in muddy sediments present an archetypal example of a new phase that does not incorporate the sediment and grows by displacing it. Investigations by Johnson et al. (2002), Winterwerp and van Kesteren (2004) and Boudreau et al. (2005) have established that the displacement of the sediment by the free gas is accomplished both by elastic expansion and by fracture, and not by fluid flow of the sediment. The result is a bubble best described as a “corn flake” (Bjorn Sundby, personal communication, McGill University, 2004), as illustrated by the computerized tomography (CT) scans in Figure 4.7, as opposed to the familiar spherical (or near-spherical) bubbles in fluids. Similar bubbles of eccentric shape can be obtained by injecting gas with a needle into gelatin, another soft solid (see Figure 4.8).

The idea that the bubbles in Figures 4.7 and 4.8 result from elasticity and fracture is supported by the application of linear elastic fracture mechanics (LEFM). Specifically, LEFM first assumes a linear Hookean constitutive equation for sediments, i.e., Equations 4.7, 4.8, 4.9, 4.10, 4.11, 4.12, 4.13, 4.14, 4.15, 4.16, 4.17, 4.18, 4.19, 4.20, and 4.21, for which we have values of E (Table 4.2) and ν (Table 4.3). Next, LEFM treats a bubble as a “coin shaped” or oblate spheroidal

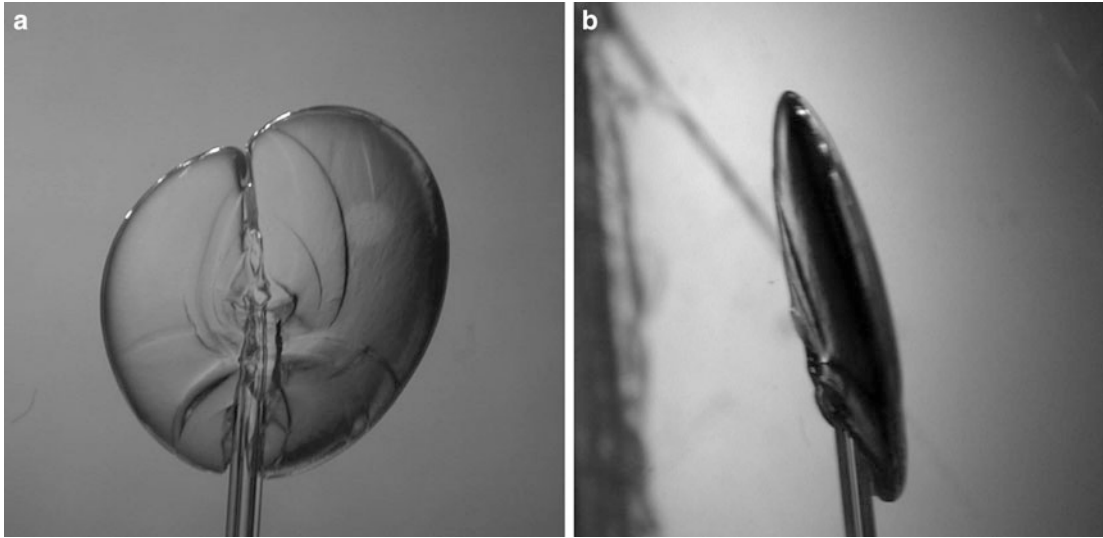


Figure 4.8. Photographs of a bubble injected into gelatin, *left* plane view (a) and *right* (b) cross section. This bubble is a thin oblate spheroid (from Johnson et al., 2002, reproduced with the kind permission of Elsevier B.V).

flaw in a thick (plane strain) medium. Given these reasonable assumptions, then the inverse of the aspect ratio, b/a , of the bubble should be given by the formula (Barry et al., 2010).

$$\frac{b}{a} = \frac{4P(1 - \nu^2)}{\pi E} \quad (\text{Eq. 4.25})$$

where b is half the length of the minor axis of the oblate spheroid, a is half the length of the major axis, and P is the internal gas pressure in excess of the surrounding ambient pressure, i.e., the stress that creates the deformation. Equation 4.25 is a similarity relation in that the aspect ratio is fixed for given combinations of ν , E and P . Figure 4.9 compares the observed inverse aspect ratio (IAR) of real bubbles in cohesive sediments and gelatin of various strengths with the predicted ratios from Equation 4.25; the agreement between observation and theory is solid, considering the errors in these measurements and the approximate nature of the theory.

Gardiner et al. (2003) and Algar and Boudreau (2009, 2010) have coupled the mechanical model for a bubble given above with a reaction-transport model for methane in porewaters to obtain predictions of the initial rate of growth of natural bubbles. Figure 4.10 illustrates the predicted initial growth rates for the conditions at Cape Lookout Bight, South Carolina, USA (see Martens and Klump, 1980; Martens and Albert, 1995). Bubbles at that site are about 100–200 cubic millimeters (mm^3) in volume and Figure 4.10 predicts about 4 days to grow bubbles to this initial size. Bubbles can grow much faster than this if they exploit pre-existing flaws/fractures in sediments that have lower K_{IC} values than the bulk sediment (Algar and Boudreau, 2010).

4.3.3 Methane Bubble Rise

If a bubble grows to a critical size in sediments, it will begin to rise due to a (pseudo-) buoyant force (Weertman, 1971a, b) from the difference in overall pressure between the top and the bottom of the bubble. While the formation and growth of a bubble in sediments can be treated as entirely an elastic process, rise must take into account more of the full dynamics of the sediment (Algar, 2009); in particular, the control of bubble rise should include a time

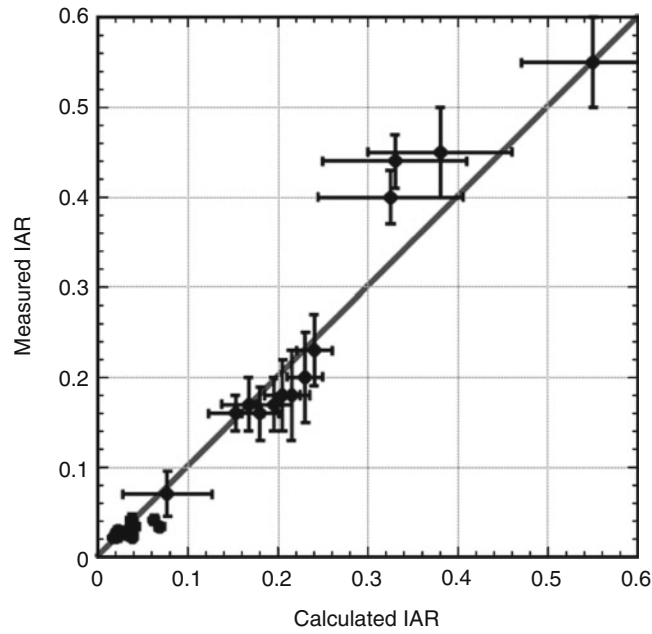


Figure 4.9. A plot of the predicted, Equation 4.10, and observed IAR of bubbles in gelatin of various strengths and in sediments. The *black line* is a 1:1 relationship (from Barry et al., 2010, reproduced with the kind permission of the American Geophysical Union).

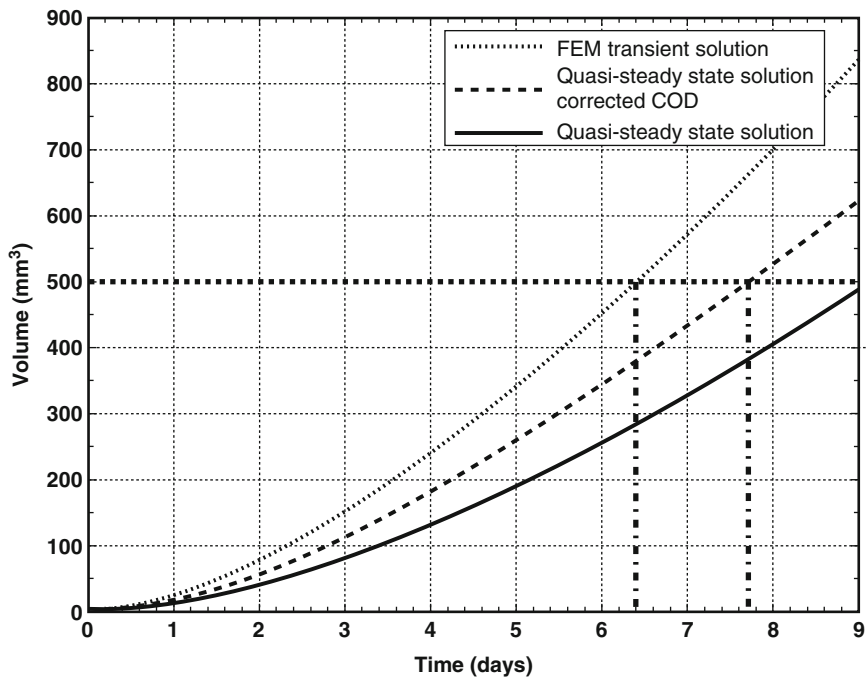


Figure 4.10. The predicted initial growth rate of a bubble in sediments from Cape Lookout Bight, North Carolina, USA. The curve labeled “FEM transient solution” is the best prediction for a sediment without a previous bubble-created flaw (from Algar and Boudreau, 2009, reproduced with the kind permission of Elsevier B.V).

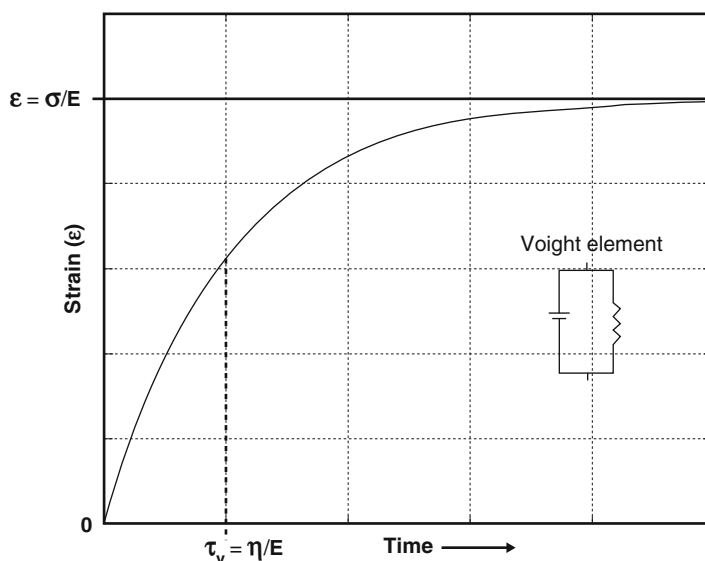


Figure 4.11. Illustration of the time behavior of a Voigt-solid, a model used to explain the rise of bubbles in sediments (Algar, 2009).

dependency from the visco-elasticity of the sediment. Thus, the speed of rise may be controlled by the rate at which sediment moves out of the way of the propagating crack, i.e., the bubble. A model of bubble rise can be based on a Voigt material, Equation 4.3; in such a material the elastic response is dampened by viscosity, such that the stress response is now time dependent. This can be represented schematically by a spring and damper (dashpot) connected in parallel (Figure 4.11). (Note that the viscous behavior of the sediment does not enter the bubble growth model because the overall time scale for growth appears to be long compared to the viscous response time. Thus, growth can be represented as an elastic equilibrium process, but the time scale of the viscous response seems to be essential to the much shorter rise process.)

Figure 4.12 illustrates time lapsed images of a simulation of a bubble rising in a cohesive sediment, where the false colors indicates the strength of the stress field from a solution of Equations 4.7, 4.8, 4.9, 4.10, 4.11, 4.12, 4.13, 4.14, 4.15, 4.16, 4.17, 4.18, 4.19, 4.20, and 4.21, including the lithostatic and hydrostatic components. The added concentration of stress at the bubble top tip, which drives the upward fracture, is clearly evident. Depending on the assumed sediment viscosity (Table 4.1), this bubble rises at a speed between 0.02 and 47 cm s^{-1} (Algar, 2009). These rapid rise speeds explain why bubble fluxes from sediments can be substantial.

Rising bubbles feedback into the chemistry of sediments by promoting the exchange of porewaters and overlying waters (e.g., Haeckel et al., 2007) and facilitating the release of volatile substances from porewaters (e.g., Yuan et al., 2007). Bubbles also can transport sediment grains, and their associated contaminants from within sediments to the sediment-water interface (Klein, 2006).

4.3.4 Animal Motion in Sediments

Infauna (i.e., the animals that live in sediments) profoundly affect the properties of sediments and the distribution of sediment components by feeding, burrowing, tube building, etc. The resulting mixing is known as bioturbation.

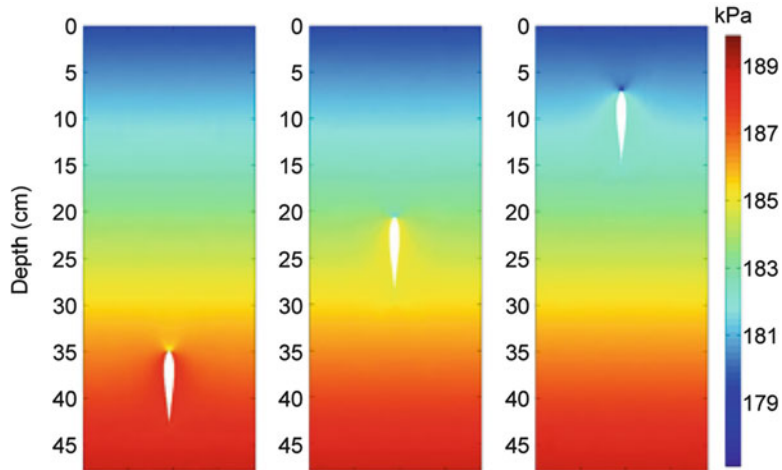


Figure 4.12. Time-lapsed illustrations of the rise of a bubble in sediments with characteristics similar to those at Cape Lookout Bight, North Carolina, USA. The color indicates the stress field, including the lithostatic load. Note the concentration of stress at the top tip of the bubble and the relaxation at the tail. The top stress propagates the bubble fracture upward (from Algar et al., 2011, reproduced with the kind permission of the American Geophysical Union).

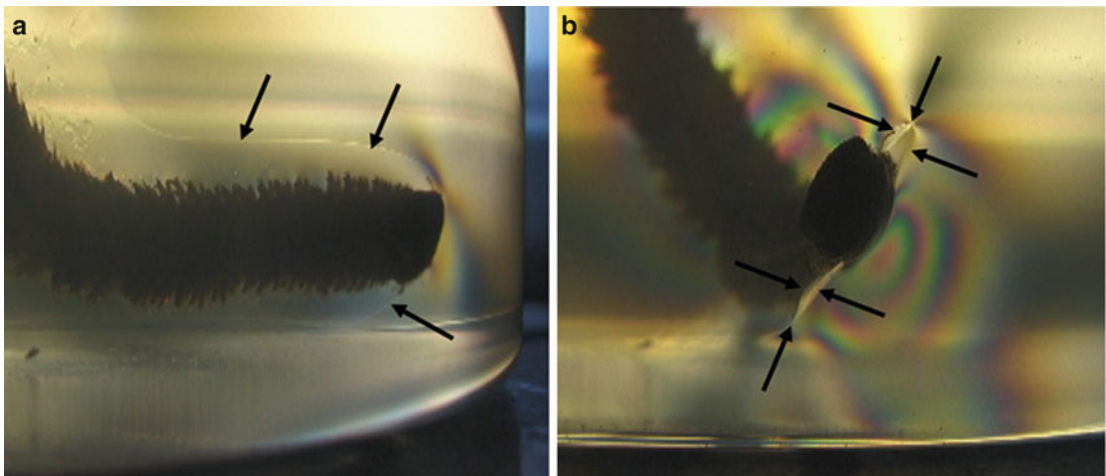


Figure 4.13. Photographs of a polychaete (*Nereis* sp.) burrowing in gelatin by propagating a fracture. The lateral and front edges of the fracture are indicated by the *black arrows* (from Dorgan et al., (2005), reproduced with the kind permission of the Nature Publishing Group/Macmillan Publishing Ltd).

As with bubbles, animal motion requires the displacement of the sediment. Dorgan et al. (2005) have shown that some organismal motions are accomplished by fracture and elastic displacement of the sediment. For example, the fracture created and propagated by a burrowing polychaete is visualized in Figure 4.13. The animal in this figure has been placed in a glass tank that contains gelatin, and the tank has been placed between a light source and a receiver (i.e., a camera). A polarizing filter has been placed between the light source and the tank and in front of the camera. The only way light reaches the camera is if the gelatin is

stressed (i.e., acts as a solid) and alters the path of the light. The amount of light deviation is proportional to the degree of stress, and that is captured by the extent of the birefringence in Figure 4.13.

The edge of the crack being propagated by the polychaete is indicated by the black arrows in Figure 4.13. The cross section (Figure 4.13b) of the crack is identical to that of a bubble (Figure 4.8). The crack is, however, not coin shaped, but elongate; as such, it is formally known as an “edge” crack. Nevertheless, its shape is also consistent with LEFM.

The creation of tubes and feeding tracts in sediments leads to the transport of both solutes and solids within sediments. The creation of a crack-based worm burrow may not initially suggest significant animal-mediated transport of solids, but the animals create the burrows to expose food particles on the burrow walls; the latter are removed, ingested and defecated elsewhere in the sediment, creating bio-mediated mixing (e.g., Boudreau, 1997; Thibodeaux et al., 2001). This mode of mixing is directly related to how animals deal with the mechanical properties of sediments.

The fact that infaunal burrows and tubes also persist in sediments, at least for some periods of time, can enhance the exchange of porewaters, as first discovered by Aller (1980, 1982). This persistence is partly due to the mechanical properties of sediments. The persistence of tubes and burrows is also attributable to organic lining, shells embedded in the wall of the tubes, etc., and the continual presence of animals. Persistent tubes invaginate the sediment-water interface, and animal ventilation of the tubes means that tube water are exchanged, with some frequency, with overlying water. This means that porewater solutes need not diffuse vertically to the sediment surface to be released, but also may move laterally into tubes. Likewise, solutes in the overlying water, e.g., oxygen, can penetrate far deeper into such sediments because of irrigated tubes.

4.4 SUMMARY

The aim of this chapter has been to highlight the mechanics (stress-strain response) of cohesive soft sediments. The apparent “softness” of such sediments, characterized by the ease one can deform them with one’s fingers, has generated the mistaken notion that such sediment are probably best considered to be a fluid. However, actual stress-strain studies show that cohesive sediment behavior is complex and often better described as a Hookean solid that is capable of fracture. Many phenomena in soft, cohesive sediments, e.g., compaction, bubble formation and rise, and animal burrowing, can only be explained via an elastic or visco-elastic model of sediment behavior, regardless of preconceptions or biases towards fluid descriptions.

ACKNOWLEDGMENTS

We would like to thank our partners-in-crime over the years, Bruce Gardiner (The University of Western Australia), Peter Jumars (The University of Maine), Kelly Dorgan (Scripps Institution of Oceanography, California), Yoko Furukawa (Naval Research Laboratory [NRL]), and Allan Reed (NRL) for sharing their inspiration and understanding. This work was supported by Natural Sciences and Engineering Research Council of Canada and U.S. Office of Naval Research. We also thank our reviewers for their considered comments. While we might not always have made the desired changes, we appreciate the opportunity to think about these issues.

REFERENCES

- Algar CK. 2009. Bubble Growth and Rise in Soft Fine-Grained Sediments. PhD Dissertation, Dalhousie University, Canada. 137 p.
- Algar CK, Boudreau BP. 2009. Transient growth of an isolated bubble in muddy, fine-grained sediments. *Geochim Cosmochim Acta* 73:2581–2591.
- Algar CK, Boudreau BP. 2010. The stability of bubbles in a linear elastic medium: Implications for bubble growth in marine sediments. *J Geophys Res - Earth Surface* 115, F03012, doi:[10.1029/2009JF001312](https://doi.org/10.1029/2009JF001312), 2010.
- Algar CK, Boudreau BP, Barry MA. 2011. Initial rise of bubbles in cohesive sediments by a process of viscoelastic fracture. *J Geophys Res – Solid Earth* 116, B04207, doi:[10.1029/2010JB008133](https://doi.org/10.1029/2010JB008133).
- Aller RC. 1980. Quantifying solute distributions in the bioturbated zone of marine sediments by defining an average microenvironment. *Geochim Cosmochim Acta* 44:1955–1965.
- Aller RC. 1982. The effects of macrobenthos on chemical properties of marine sediment and overlying water. In McCall PL, Tevesz MJS, eds, *Animal-Sediment Interactions*. Plenum Publishing Corporation, New York, NY, USA, pp 53–102.
- Aluko OB, Chandler HW. 2006. A fracture strength parameter for brittle agricultural soils. *Biosyst Eng* 93:245–252.
- Barry MA. 2010. Elastic and Fracture Behaviour of Marine Sediment in Response to Free Gas. PhD Dissertation, Dalhousie University, Canada. 177 p.
- Barry MA, Boudreau BP, Johnson BD, Reed AH. 2010. Validation of bubble growth by LFM in sediments and other soft elastic solids. *J Geophys Res – Earth Surface* 115, F04029, doi:[10.1029/2010JF001833](https://doi.org/10.1029/2010JF001833).
- Barry MA, Johnson BD, Boudreau BP. 2012. A new instrument for high-resolution *in situ* assessment of Young's modulus in shallow cohesive sediments. *Geo-Mar Lett* doi: [10.1007/s00367-012-0277-z](https://doi.org/10.1007/s00367-012-0277-z).
- Been K, Sill GC. 1981. Self-weight consolidation of soft soils: An experimental and theoretical study. *Géotechnique* 31:519–535.
- Bennett RH, Bryant WR, Hulbert MH, eds. 1991. *Microstructure of Fine-Grained Sediments – from Shale to Mud*. Springer-Verlag, New York, NY, USA. 582 p.
- Bennett RH, Hulbert MH, Meyer MM, Lavoie DM, Briggs KB, Lavoie DL, Baerwald RJ, Chiou WA. 1996. Fundamental response of pore-water pressure to microfabric and permeability characteristics: Eckernförde Bay. *Geo-Mar Lett* 16:182–188.
- Bennett RH, Kastner M, Baerwald RJ, Ransom B, Sawyer W, Lambert MW, Olsen H, Hulbert MH. 1999. Early diagenesis: Impact of organic matter on mass physical properties and processes, California continental margin. *Mar Geol* 159:7–34.
- Berner RA. 1971. *Principles of Chemical Sedimentology*. McGraw-Hill, New York, NY, USA. 240 p.
- Berner RA. 1980. *Early Diagenesis: A Theoretical Approach*. Princeton University Press, Princeton, NJ, USA. 241 p.
- Best AI, Richardson MD, Boudreau BP, Judd AG, Leifer I, Lyons AP, Martens CS, Orange DL, Wheeler SJ. 2006. Shallow seabed methane gas could pose coastal hazard. *EOS: Trans Amer Geophys Union* 87:213–217.
- Biot MA. 1941. General theory of three-dimensional consolidation. *J Appl Phys* 12:155–164.
- Biot MA. 1956. General solutions of the equations of elasticity and consolidation for a porous material. *J Appl Mech* 23:91–96.
- Biot MA. 1973. Nonlinear and semilinear rheology of porous solids. *J Geophys Res* 78: 4924–4937.

- Bird RB, Stewart WE, Lightfoot EN. 2007. *Transport Phenomena*, 2nd ed. John Wiley & Sons, New York, NY, USA. 920 p.
- Boudreau BP. 1996. The diffusive tortuosity of fine-grained unlithified sediments. *Geochim Cosmochim Acta* 60:139–3142.
- Boudreau BP. 1997. *Diagenetic Models and their Implementation*. Springer-Verlag, Berlin, Germany. 414 p.
- Boudreau BP, Algar C, Johnson BD, Croudace I, Reed A, Furukawa Y, Dorgan KM, Jumars PA, Grader AS, Gardiner BS. 2005. Bubble growth and rise in soft sediments. *Geol* 33:517–520.
- Boudreau BP, Bennett RH. 1999. New rheological and porosity equations for steady-state compaction. *Am J Sci* 299:517–528.
- Boudreau BP, Meysman FJR. 2006. Predicted tortuosity of muds. *Geol* 34:693–696.
- Breitzke M. 2006. Physical properties of marine sediments. In Schultz HD, Zabel M, eds, *Marine Geochemistry*, 2nd ed. Springer, Berlin, Germany, pp 27–71.
- Broek D. 1982. *Elementary Engineering Fracture Mechanics*. Narinus Nijhoff, Boston, MA, USA. 469 p.
- Burdige DJ. 2006. *Geochemistry of Marine Sediments*. Princeton University Press, Princeton, NJ, USA. 609 p.
- Clayton CRI, Heymann G. 2001. Stiffness of geomaterials at very small strains. *Geotech* 51:245–255.
- Craig RF. 2004. *Craig's Soil Mechanics*. Taylor and Francis, London, United Kingdom. 464 p.
- Das BM. 2008. *Advanced Soil Mechanics*. Taylor and Francis, London, United Kingdom. 600 p.
- Davis AM, Schultheiss PJ. 1980. Seismic signal processing in engineering-site investigation – a case history. *Ground Eng* 13:44–48.
- Davis RO, Selvadurai APS. 1996. *Elasticity and Geomechanics*. Cambridge University Press, Cambridge, United Kingdom. 256 p.
- Davis RO, Selvadurai APS. 2002. *Plasticity and Geomechanics*. Cambridge Univ. Press, Cambridge, United Kingdom. 304 p.
- de Boer R. 1992. Development of porous media theories - A brief historical review. *Transp Porous Media* 9:155–164.
- DiToro DM. 2001. *Sediment Flux Modeling*. Wiley-Interscience, New York, NY, USA. 624 p.
- Dorgan KM, Jumars PA, Johnson BD, Boudreau BP, Landis E. 2005. Burrow elongation by crack propagation. *Nat* 433:475.
- Engelhardt WV, Gaida KH. 1963. Concentration changes of pore solutions during the compaction of clay sediments. *J Sed Pet* 33:919–930.
- Gardiner BS, Boudreau BP, Johnson BD. 2003. Growth of disk-shaped bubbles in sediments. *Geochim Cosmochim Acta* 67:1485–1494.
- Gasparre A, Nishimura S, Minh NA, Coop MR, Jardine RJ. 2007. The stiffness of natural London clay. *Géotech* 57:33–47.
- Gibson RE. 1958. The progress of consolidation in a clay layer increasing in thickness with time. *Géotechnique* 8:171–182.
- Gibson RE, Schiffman RL, Whitman RV. 1989. On two definitions of excess pore pressure. *Géotechnique* 39:169–171.
- Giles MR. 1997. *Diagenesis: A Quantitative Perspective*. Kluwer Academic Publisher, Dordrecht, The Netherlands. 526 p.
- Gross D, Seelig T. 2006. *Fracture Mechanics*. Springer-Verlag, Berlin, Germany. 319 p.
- Haeckel M, Boudreau BP, Wallmann K. 2007. Bubble-induced porewater irrigation: A 3-D model for porewater mixing. *Geochim Cosmochim Acta* 71:5135–5154.
- Hall TJ, Bilgen M, Insana MF, Krouskop TA. 1997. Phantom materials for elastography. *IEEE Transactions on Ultrasonics, Ferroelectrics, and Frequency Control* 44:1355–1365.

- Hamilton EL. 1971. Elastic properties of marine sediments. *J Geophys Res* 76:579–604.
- Hamilton EL. 1979. v_p/v_s and poisson's ratios in marine sediments and rocks. *J Acoust Soc Am* 66:1093–1101.
- Hamilton EL, Bucker HP, Keir DL, Whitney JA. 1970. Velocities of compressional and shear waves in marine sediments determined from a research submersible. *J Geophys Res* 75:4039–4049.
- Hsiao SV, Shemdin OH. 1980. Interaction of ocean waves with a soft bottom. *J Phys Oceanogr* 10:605–611.
- Hunter RJ. 2001. *Foundations of Colloid Science*, 2nd ed. Oxford University Press, Oxford, United Kingdom. 806 p.
- Jaeger JC. 1969. *Elasticity, Fracture and Flow, with Engineering and Geological Applications*. Chapman and Hall, London, United Kingdom. 268 p.
- Jiang F, Mehta A. 1995. Mudbanks of the southwest coast of India IV: Mud viscoelastic properties. *J Coastal Res* 11:918–926.
- Johnson BD, Boudreau BP, Gardiner BS, Maass R. 2002. Mechanical response of sediments to bubble growth. *Mar Geol* 187:247–363.
- Johnson BD, Barry M, Boudreau BP, Jumars PA, Dorgan KM. 2012. Profiling fracture toughness in cohesive sediments. *Geo-Mar Lett* 32:39–48, doi: [10.1007/s00367-011-0243-1](https://doi.org/10.1007/s00367-011-0243-1)
- Klein S. 2006. Sediment porewater exchange and solute release during ebullition. *Mar Chem* 102:60–71.
- Koppula SD, Morgenstern NR. 1982. On the consolidation of sedimenting clays. *Can Geotech J* 19:260–268.
- Lavoie D, Griffin SR, Grosz FB. 1996. DIAS - A novel technique for measuring *in situ* shear modulus. *Geo-Marine Lett* 16:254–260.
- Lee K, Sills GC. 1981. The consolidation of a soil stratum, including self-weight effects and large strains. *Int J Num Anal Meth Geomech* 5:405–428.
- L'Esperance JC. 2009. Simultaneous measurement of Young's modulus and Poisson's ratio of marine sediments with a simple uni-axial compression test. MSc Thesis, Dalhousie University, Canada. 218 p.
- Long RR. 1961. *Mechanics of Solids and Fluids*. Prentice-Hall, Engelwood Cliffs, NJ, USA. 156 p.
- Maa P-Y. 1986. *Erosion of Soft Mud by Waves*. PhD Dissertation, University of Florida, Gainesville, FL, USA. 286 p.
- Maa P-Y, Mehta AJ. 1988. Soft mud properties: Voigt model. *J Waterw Port Coast Ocean Eng* 114:634–650.
- Markidou A, Shih WY, Shih W-H. 2005. Soft-materials elastic and shear moduli measurement using piezoelectric cantilevers. *Rev Sci Instrum* 76:064302; doi:[10.1063/1.1928407](https://doi.org/10.1063/1.1928407).
- Martens CS, Albert DB. 1995. Biogeochemical processes controlling concentrations and transport of biogenic methane in organic rich coastal sediments. In Wever TF, ed, *Proceedings of the Workshop on Modeling Methane-Rich Sediments of Eckernforde Bay, Eckernforde, June 26–30, Forschungs Bundeswehr Wasserschall Geophysik*, pp 10–17.
- Martens C, Klump J. 1980. Biogeochemical cycling in an organic-rich coastal marine basin-1. Methane sediment-water exchange processes. *Geochim Cosmochim Acta* 44:471–490.
- McNabb A. 1960. A mathematical treatment of one-dimensional consolidation. *Q Appl Math* 17:337–347.
- Mehta AJ, Partheniades E. 1982. Resuspension of deposited cohesive sediment beds. *Proceedings 18th Coastal Engineering Conference*, v. 2, Cape Town, South Africa, pp 1569–1588.
- Menand T, Tait S. 2002. The propagation of a buoyant liquid-filled fissure from a source under constant pressure: an experimental approach. *J Geophys Res* 107:2306; doi:[10.1029/2001JB000589](https://doi.org/10.1029/2001JB000589).

- Mitchell JK, Soga K. 2005. *Fundamentals of Soil Behaviour*, 3rd ed. Wiley, New York, NY, USA. 577p.
- Partheniades E. 1991. Effect of bed shear stresses on the deposition and strength of deposited cohesive muds. In Bennett RH, Bryant WR, Hulbert MH, eds, *Microstructure of Fine-grained Sediments: From Mud to Shale*. Springer Verlag, Berlin, Germany, pp 175–183.
- Pickering DJ. 1970. Anisotropic elastic parameters for soil. *Géotechnique* 20:271–276.
- Raju LV, Ramana YV. 1986. Physical and elastic properties of marine sediments off Bombay. *Indian Mar Geotechnol* 6:359–375.
- Rieke HH, Chilingarian GV. 1974. *Compaction of Argillaceous Sediments*. Elsevier, Amsterdam, The Netherlands. 424 p.
- Rivalta E, Dahm T. 2006. Acceleration of buoyancy-driven fractures and magmatic dikes beneath the free surface. *Geophys J Int* 166:1424–1439.
- Salem HS. 2000. Poisson's ratio and the porosity of surface soils and shallow sediments, determined from seismic compressional and shear wave velocities. *Géotech* 50:461–463.
- Sato H, Katano M, Takigawa T, Masuda T. 2001. Estimation for the elasticity of vascular endothelial cells on the basis of atomic force microscopy and Young's modulus of gelatin gels. *Polymer Bull* 47:375–381.
- Schulz HD, Zabel M. 2006. *Marine Chemistry*, 2nd ed. Springer, Berlin, Germany. 574 p.
- Shames IH. 1964. *Mechanics of Deformable Solids*. Prentice-Hall, Englewood Cliffs, NJ, USA. 532 p.
- Small JC, Booker JR, Davis EH. 1976. Elasto-plastic consolidation of soil. *Int J Solids Struct* 12:431–448.
- Takada A. 1990. Experimental study on propagation of liquid-filled crack in gelatin: Shape and velocity in hydrostatic stress condition. *J Geophys Res* 95:8471–8481.
- Terzaghi K. 1943. *Theory of Soil Mechanics*. John Wiley and Sons, New York, NY, USA. 510 p.
- Thibodeaux LJ, Valsaraj KT, Reible DD. 2001. Bioturbation-driven transport of hydrophobic organic contaminants from bed sediment. *Environ Eng Sci* 18:215–233.
- Timoshenko SP, Goodier JN. 1934. *Theory of Elasticity* (1970 printing). McGraw-Hill, New York, NY, USA. 567 p.
- Toorman EA. 1996. Sedimentation and self-weight consolidation: general unifying theory. *Géotechnique* 46:103–113.
- Verreet G, Berlamont J. 1988. Rheology and non-Newtonian behavior of sea and estuarine mud. In Cheremisinoff NP, ed, *Encyclopedia of Fluid Mechanics*. Gulf Publishing Company, Houston, TX, USA, pp135–149.
- Wang HF. 2000. *Theory of Linear Poroelasticity with Applications to Geomechanics and Hydrology*. Princeton University Press, Princeton, NJ, USA. 287 p.
- Weertman J. 1971a. Theory of water-filled crevasses in glaciers applied to vertical magma transport beneath oceanic ridges. *J Geophys Res* 76:1171–1183.
- Weertman J. 1971b. Velocity at which liquid-filled cracks move in the Earth's crust or in glaciers. *J Geophys Res* 76:8544–8553.
- Williams PR, Williams DJA. 1989. Rheometry for concentrated cohesive suspensions. *J Coastal Res* 5:151–164.
- Winterwerp JC, van Kesteren WGM. 2004. Introduction to the Physics of Cohesive Sediment in the Marine Environment, *Developments in Sedimentology* 56. Elsevier, Amsterdam, The Netherlands. 466 p.
- Yong RN, Warkentin BP. 1966. *Introduction to Soil Behavior*. Macmillan, London, UK. 451 p.
- Yuan Q, Valsaraj KT, Reible DD, Willson CS. 2007. A laboratory study of sediment and contaminant release during gas ebullition. *J Air Waste Manag Assoc* 57:1103–1111.
- Znidarcic D, Schiffman RL. 1982. On Terzaghi's concept of consolidation. *Géotechnique* 32: 387–389.

APPENDIX 4A

If a material is mapped (each point given a coordinate), then deformed, and the same points in the medium remapped, the resulting change in the position of an arbitrary point is called its displacement vector, u . The spatial derivatives of the displacement define the strain tensor, ε . Formally,

$$\varepsilon = \frac{1}{2} [\nabla u + (\nabla u)^T] \quad (\text{Eq. 4.A1})$$

where \mathbf{u} is the displacement gradient matrix and the superscript T indicates the transpose. Thus, the tensile/compressive strain that occurs in the x direction is given by

$$\varepsilon_{xx} = \frac{\partial u_x}{\partial x} \quad (\text{Eq. 4.A2})$$

and the subscripts can be dropped for a purely one-dimensional system, e.g., steady-state sediment compaction.